

# Transition from localized to delocalized trajectories in random walk subject to random drives

Zijun Li\* and Jiming Yang\*

*Zhixin High School, Guangzhou, Guangdong, China*

Huiyu Li

*Atlas Science, Princeton, New Jersey, USA*

(Dated: November 22, 2023)

Random walk subject to random drive has been extensively employed as a model for physical and biological processes. While equilibrium statistical physics has yielded significant insights into the distributions of dynamical fixed points of such a system, its non-equilibrium properties remain largely unexplored. In contrast, most real-world applications concern the dynamical aspects of this model. In particular, dynamical quantities like heat dissipation and work absorption play a central role in predicting and controlling non-equilibrium phases of matter. Recent advances in non-equilibrium statistical physics enable a more refined study of the dynamical aspects of random walk under random drives. We perform a numerical study on this model and demonstrate that it exhibits two distinct phases: a localized phase where typical random walk trajectories are non-extensive and confined to the neighborhood of fixed points, and a delocalized phase where typical random walk trajectories are extensive and can transition between fixed points. We propose different summary statistics for the heat dissipation and show that these two phases are distinctly different. Our characterization of these distinctive phases deepens the understanding of and provides novel strategies for the non-equilibrium phase of this model.

## I. INTRODUCTION

Recent advances in non-equilibrium statistical physics [1–3] have shifted the focus from properties of equilibrium states to the thermodynamic analysis of transient properties in a system’s history. Heat dissipation, or entropy production, has provided significant insights into the understanding and control of non-equilibrium phases of matter, with notable applications in biological processes such as self-assembly and self-replication [4–10]. It has been hypothesized that, given the same physical configuration space, living systems are more likely to exhibit high dissipation trajectories compared to non-living systems. Such self-organization phenomena, named *dissipative adaptation* [11], have been studied in the context of many-body systems driven out-of-equilibrium [12–16]. Therefore, understanding and quantifying physical conditions that lead to high dissipation is important. In this paper, we study dissipation in the model of random walk subject to random drives, a model extensively used for diffusion processes [17, 18], active matter [19–21], and directed movements in biology [22, 23]. While equilibrium statistical physics has provided significant insights into the distributions of dynamical fixed points of such a system [18], its non-equilibrium properties remain largely unexplored.

Through a detailed numerical analysis, we uncover two contrasting phases within this model: a localized phase, characterized by non-extensive, confined random walk paths near fixed points, and a delocalized phase, marked

by extensive random walk paths with the ability to move between fixed points. Similar localization-delocalization transitions have been discussed in the context of large deviation theory in various settings, from random media [24, 25] to random graphs [26–29] and quantum systems [30, 31]. We introduce various summary statistics to analyze heat dissipation and establish the distinct nature of these two phases. This exploration provides a novel numerical strategy to characterize the localization-delocalization phase transition in this model, and offers innovative approaches for studying its non-equilibrium behavior.

Our paper is organized as follows: In Section II we introduce the Langevin equation for random walk and motivate the model for its random drive. In Section III we introduce the vector field model for the random drive and discuss the Metropolis algorithm for simulating it. In Section IV we combine the Langevin equation and vector field to study random walk under random drive and discuss different regimes of the model. Finally, in Section V we propose different metrics for detecting these two phases and demonstrate that the behavior of these metrics is distinctly different in the two phases.

## II. LANGEVIN SYSTEM

The original Langevin equation [32] describes Brownian motion, the apparently random movement of a particle in a fluid due to collisions with the molecules of the fluid,

$$m \frac{dv}{dt} = -\gamma v + \eta(t). \quad (1)$$

\* Equal contribution.

Here,  $v$  is the velocity of the particle, and  $m$  is its mass. The force acting on the particle is written as a sum of a viscous force proportional to the particle's velocity (Stokes's law), and a noise term  $\eta(t)$  representing the effect of the collisions with the molecules of the fluid. The force  $\eta(t)$  has a Gaussian probability distribution with the correlation function

$$\langle \eta_i(t) \eta_j(t') \rangle = 2\gamma k_B T \delta_{ij} \delta(t - t'). \quad (2)$$

However, the Langevin equation is used to describe the motion of a "macroscopic" particle at a much longer time scale. In our research, we are going to study the Langevin model in the regime that particles are moving in an extremely sticky fluid with low Reynold's number. In this limit, we can consider the system as a non-inertial system. In such non-inertial system, acceleration can be neglected. In this limit, the original Langevin equation is transformed into

$$-\gamma \dot{\vec{x}} + F(\vec{x}) + \eta(t) = 0. \quad (3)$$

Here, Eq.3 describes a general overdamped Langevin system with many degrees of freedom  $\vec{x}$ .  $F(\vec{x})$  models the complicated external drivings that depends on the coordinate  $\vec{x}$ . We can further decompose  $F$  into two components,  $F(\vec{x}) = F_{ext}(\vec{x}) - \nabla U_{int}(\vec{x})$ .  $F_{ext}(\vec{x})$  is the external drive force that the particle experiences, and  $U_{int}(\vec{x})$  is the internal potential that the particles live in and models the internal dynamics of the system. For simplicity, in the following we consider the case with  $U_{int}(\vec{x}) = 0$  and focus on the effect of the external drive. Therefore, the Langevin system of interest is

$$\gamma \dot{\vec{x}} = F_{ext}(\vec{x}) + \eta(t). \quad (4)$$

In many applications of the model 4,  $F_{ext}$  is most relevant when it models a random external drive with strong correlation within nearby coordinates  $\vec{x}$ . In general, we require that

$$\langle F_{ext}(\vec{x}) F_{ext}(\vec{x}') \rangle \sim e^{-\frac{|\vec{x} - \vec{x}'|}{\xi}}, \quad (5)$$

where  $\xi$  is the correlation length within the model.

### III. MASSIVE VECTOR FIELD

Eq.5 is observed in many statistical models away from critical points. In particular, we propose to use the massive vector field, which is a much studied model in both high energy physics [33] and statistical physics [34]. It is also widely employed as model of phase transition in the Ginzburg-Landau theory.

#### A. The model

We consider a system of vectors  $\vec{A}$  in a flat background with the Hamiltonian:

$$H[\vec{A}] = \frac{1}{2} J |\nabla \vec{A}|^2 + \frac{1}{2} m^2 |\vec{A}|^2. \quad (6)$$

$H[\vec{A}]$ , the Hamiltonian, describes the total energy of the vector field. The first term stands for its kinetic energy, which measures the cooperativity of the vectors, and  $J$  describes the interaction strength. The second term is called the mass term, in which  $m$  stands for the mass of the vectors, which measures the randomness of the vectors. To see this, note that in the limit when  $J = 0$ , the equilibrium distribution of Eq.6 is

$$p[\vec{A}]|_{J=0} \sim \exp \left\{ -\beta H[\vec{A}] \right\} = \exp \left\{ -\frac{1}{2} m^2 |\vec{A}|^2 \right\}, \quad (7)$$

where  $\beta$  is the inverse temperature. To gain more physical intuition, we can compare our vector field model with the XY model[35, 36]. XY model is a  $n$ -dimensional lattice. On each lattice site there is an unit-length vector  $\vec{S}_i = (\sin \theta_i, \cos \theta_i)$ . The Hamiltonian is given by

$$H = -\frac{1}{2} J \sum_{\langle i, j \rangle} \vec{S}_i \cdot \vec{S}_j = -\frac{1}{2} J \sum_{\langle i, j \rangle} \cos(\theta_i - \theta_j) \quad (8)$$

as  $|\vec{S}_i| = |\vec{S}_j| = 1$  and  $J$  stands for the cooperativity between vectors. Our massive vector field model Eq.6 can be thought of as the continuum limit of Eq.8 with fixed vector length  $|\vec{A}| = 1$  and variable angles.

#### B. Simulation Method

In order to obtain the equilibrium configuration of Eqn.6, we use Metropolis-Hastings algorithm[37]. Metropolis-Hastings algorithm use Monte-carlo methods to obtain a sequence of random samples from a probability distribution when direct sampling is difficult. This sequence can be used to approximate the distribution. In our case, the distribution of interest is the equilibrium distribution that we would like to sample from. We focus on the case of 2-dimension because the simulation is relatively simple and the configurations are already highly non-trivial. We decompose the vector field into its horizontal and vertical components,  $\vec{A} = (A_h, A_v)$ , such that  $|\vec{A}|^2 = |A_h|^2 + |A_v|^2$ . Now Eq.6 can be written as

$$H[\vec{A}] = \frac{1}{2} J (|\nabla A_h|^2 + |\nabla A_v|^2) + \frac{1}{2} m^2 (|A_h|^2 + |A_v|^2) \quad (9)$$

We start our simulation with a normally-distributed initial conditions  $A_v$  and  $A_h$  on every lattice site, and we assume periodic boundary condition.

In Metropolis-Hastings algorithm, the probability of observing configuration  $\vec{A}$  is assumed to be Boltzmann distributed.

$$P(\vec{A}) = \frac{e^{-\beta H[\vec{A}]}}{Z} \quad (10)$$

where  $Z$  stands for partition function, and  $\beta$  stands for the thermodynamic term defined as  $1/K_B T$ .  $K_B$  stands for Boltzmann constant, and  $T$  stands for temperature.

In each Monte-Carlo sweep, we randomly pick one vector from lattice site  $\vec{x}$ ,  $\vec{A}[\vec{x}]$ , and propose a random move. After updating this specific vector, we obtain an updated configuration  $\vec{A}'$ , with associated probability  $P(\vec{A}') = e^{-\beta H[\vec{A}']}/Z$ . Now the relative probability of obtaining  $A'$  vs  $A$  is

$$r = \frac{P(\vec{A}')}{P(\vec{A})} = e^{-\beta(H[\vec{A}'] - H[\vec{A}])} \equiv e^{-\beta(\Delta H)} \quad (11)$$

where  $\Delta H = H[\vec{A}'] - H[\vec{A}]$ .

If  $\Delta H < 0$ , we always accept the change as our purpose is to acquire the ground state of the system.

If  $\Delta H > 0$ , we accept the change with probability  $r$ .

The acceptance probability is calculated as following. We generate a random number  $x$  from 0 to 1 following uniform distribution. If  $x < r$ , we accept the change. Otherwise, the change will not be applied to the specified vector and the simulation carries on to the next vector until we exhaust all the vectors in the lattice.

After a considerably large amount of Monte-Carlo sweep (see Appendix A), the vector field reaches equilibrium and we obtain a relatively lowest energy configuration. The resultant vector field is shown in Fig.1.

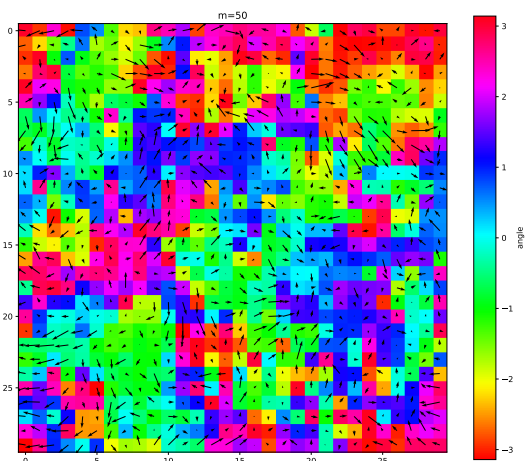


Figure 1. Example configuration of massive vector field simulated by Metropolis-Hasting algorithm. Color represents angle of the vectors from 0 to  $2\pi$ .

The arrows in the graph stand for our vectors in the vector field. The length of every arrow represents the magnitude of the force of that lattice site, and the direction of every arrow represents its direction of force. The coloring in the graph visualizes the direction of every vector. Each color represents an angle value of the vectors as the color scheme shows. Therefore, the graph can effectively visualize the alignments between nearby vectors and serves as an efficient visual aid for our simulations.

#### IV. LANGEVIN EQUATION IN A VECTOR FIELD BACKGROUND

The massive vector field  $\vec{A}$  we applied to our Langevin system has random directions and lengths, which we use as a model of the external driving force  $F_{ext}$  exerted on the Langevin particles  $\vec{x}$ .

Take a particular realization of the massive vector field as the external forces we can decompose

$$F_{ext}(\vec{x}) = \vec{A}(\vec{x}) = \left( A_h(\vec{x}), A_v(\vec{x}) \right). \quad (12)$$

Here,  $\vec{A}_h(\vec{x})$  represents the horizontal force exerted on the particles with respect to their positions. Similarly,  $\vec{A}_v(\vec{x})$  represents the vertical force exerted on the particles with respect to their positions. We can think of  $A_h$  and  $A_v$  as two independent vector fields coupled through their kinetic and mass terms (Eqn.6).

Then we put the external forces (the effect of vector field) into the Langevin equation.

$$\gamma \dot{\vec{x}} = \vec{A}(\vec{x}) + \eta(t) \quad (13)$$

We use uniform initial positions for the Langevin particles, and then let them evolve under the Langevin equation Eq.13.

We plot the trajectories of particles under the driving of the vector field, and color-code them differently for different trajectories, the results are shown in Fig.2.

When the particle passes through its trajectory, the kinetic energy will be transferred into the system when the particle overcomes viscous resistance, this energy is known as dissipation, the dissipation rate is

$$\Gamma(t) = \vec{F}_{diss}(t) \cdot \dot{\vec{x}} = \vec{A}(\vec{x}) \cdot \dot{\vec{x}}(t) \quad (14)$$

We can calculate the total dissipation energy from the particle to the system by

$$Diss = \int \Gamma(t) dt = \vec{A}(\vec{x}) \cdot \dot{\vec{x}}(t) dt \quad (15)$$

Thus, the trajectory and dissipation of a particle are only affected by the massive vector field and the random thermal motion. And then we can plot the dissipation of

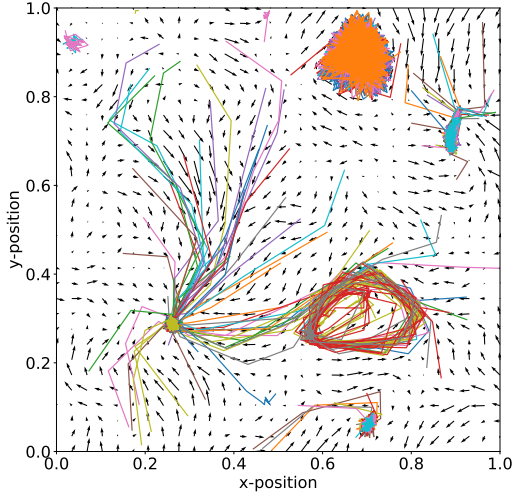


Figure 2. Example trajectories of particles moving under Eq.13. Different color represents different initial conditions of the particles.

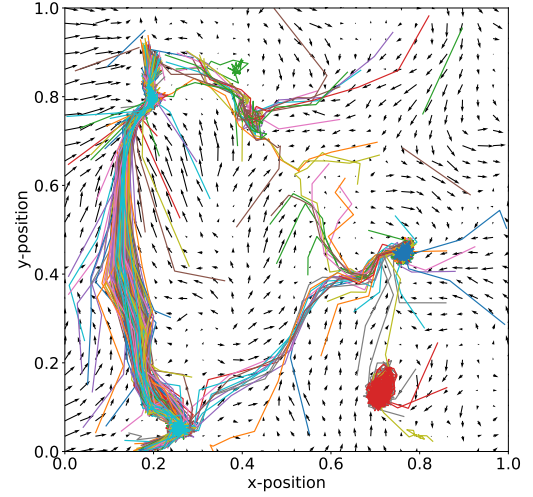


Figure 4. Example of trajectory in high dissipation condition ( $m = 10, J = 100$ )

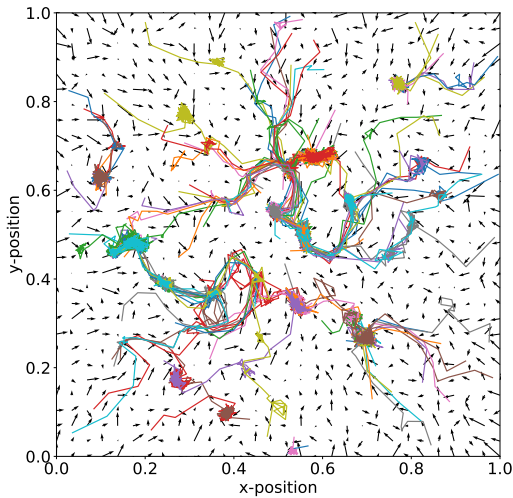


Figure 3. Example of a low dissipation trajectories ( $m = 100, J = 1$ )

each particle trajectory calculated by Eq.15 in the histogram.

Different combination of  $m$  and  $J$  results in different statistics of the vector field, and in turn affects the typical trajectories of the Langevin particles. Depending on the coordination of nearby vectors, some trajectories, Langevin particles can either get trapped into nearby attractors and limit cycles, or travel further from attractors to attractors.

One situation is that  $m \gg J$ . In this situation, as shown in Fig.3, the distribution of the vector angles is

totally random. there is not any cooperation between nearby vectors. All  $A_h(\vec{x})$  vectors and  $A_v(\vec{x})$  vectors are random and approximately Gaussianly-distributed. The majority of the trajectories get stuck at local attractors and seldom hop between nearby attractors. We define this situation as low-dissipation condition.

Another extreme situation is when  $J \gg m$ , and this corresponds to total coordination, where the vector field resembles a constant vector field. In this case, the external drive represents a constant driving force. The resulting dynamics in this regime is not interesting.

Our ideal condition is that the when  $m$  and  $J$  are comparable. In this situation, as shown in Fig.6 there are some fix points that particles get trapped into. However, at the same time, there are also extensive trajectories where particles can hop between fix points. We define this situation as high-dissipation condition.

In general, particles that have more extensive trajectories tend to have higher dissipation, as evident in Eqn.15 that total dissipation energy is proportional to the total distance traveled by the Langevin particle. Therefore, by observing the corresponding dissipation energy we can infer the trajectories of the particles in this system. Therefore, in the following we focus on the distribution of dissipation energy.

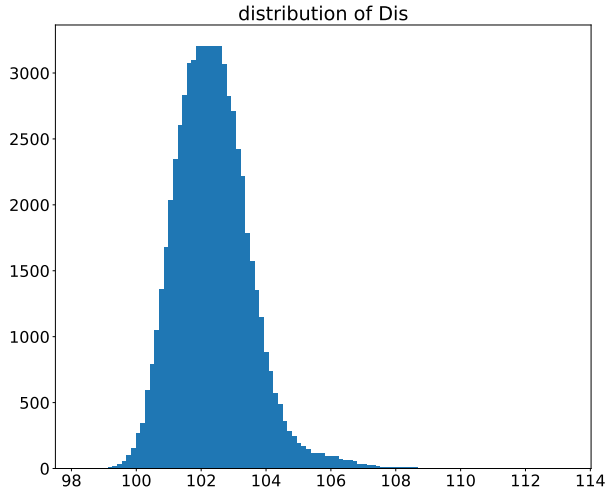


Figure 5. Example of histogram of general dissipation in low dissipation condition  $m = 100, J = 1$ )

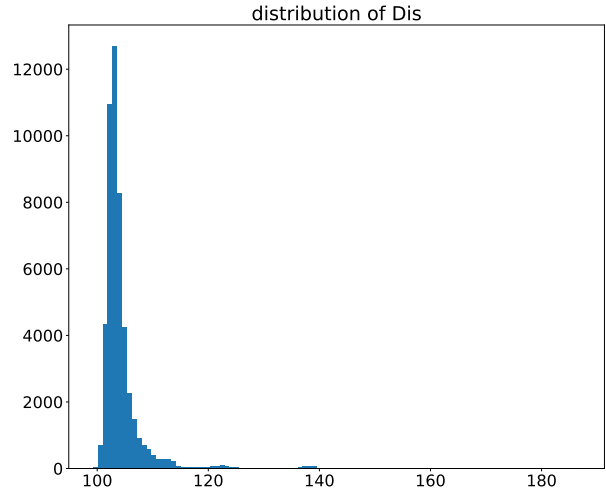


Figure 6. Example of histogram of general dissipation in high dissipation condition  $m = 10, J = 100$ )

## V. FEATURES OF LOW DISSIPATION CONDITION AND HIGH DISSIPATION CONDITION

### A. Compare Relatively Large Dissipation in Each Condition

In low-dissipation condition, the kinetic energy transferred into system is generally small since the trajectories tend to get stuck. The distribution of total dissipation of trajectories is shown in Fig.5.

In high-dissipation condition, the total dissipation is larger than in the low-dissipation condition, since particles can hop between fix points before they finally stop. The distribution of total dissipation is shown in Fig.6.

As what is shown in both Fig.5 and Fig.6 that although there are some higher dissipation in each histogram, their difference can't be detected obviously by comparing their mean value. Therefore, we need another method to present the difference between high dissipation phase and low dissipation phase. Our method is to focus on the relatively high dissipation group, which corresponds to the outlier part in the dissipation distribution.

We start with calculating the Interquatile Range (IQR) of each distribution by

$$IQR = Q3 - Q1 \quad (16)$$

Here, IQR refers to the range between the 25<sup>th</sup> percentile(Q1) and the 75<sup>th</sup> percentile(Q2) of each distribution. According to the statistical rule of defining outliers by IQR, any data that is larger than  $Q3 + 1.5IQR$  is

considered as outliers. Then, we can calculate the mean value of dissipation from the outliers

$$\langle D_{outlier} \rangle = \sum_i D_i f_i [i \in (Q3 + 1.5IQR, max)], \quad (17)$$

where  $D_i$  represents the  $i^{th}$  bin in the outlier dissipation histogram and  $f_i$  represents the frequency at this dissipation.

In the same way, we can calculate the total dissipation by

$$\langle D \rangle = \sum_j D_j f_j [j \in (min, max)] \quad (18)$$

With  $\langle D_{outlier} \rangle$  and  $\langle D \rangle$ , we can calculate their ratio by

$$Ratio = \frac{\langle D_{outlier} \rangle}{\langle D \rangle} \quad (19)$$

The ratio stands for the portion of relatively large dissipation trajectories from the overall dissipation. Hence we will have a more direct view of the difference between the comparably high dissipation part of trajectories in the two regimes. We plot this ratio in the high-dissipation condition and low-dissipation condition in Fig.7.

We can clearly see from the graph that the ratio of high dissipation phase is greater than low dissipation phase. This means that the proportion of large dissipation values is greater in high dissipation phase than in the low dissipation phase, which provides an evidence of which phase (low-dissipation vs high-dissipation) the system lives in.

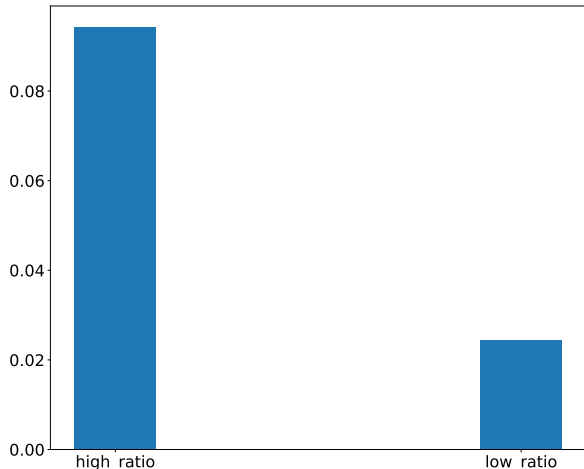


Figure 7. The two ratios of high dissipation phase and low dissipation phase

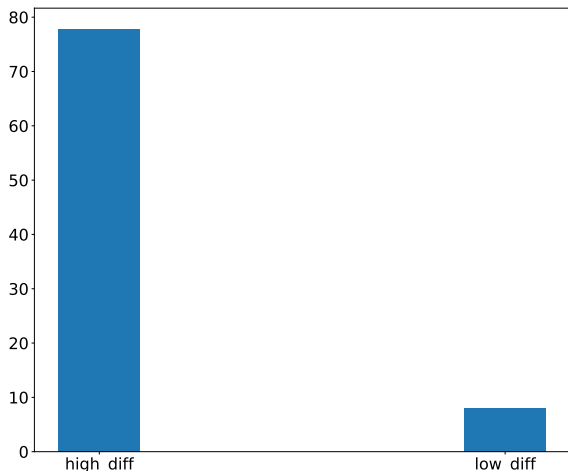


Figure 8. The range of outliers in each dissipation condition.

Also, we can use another method to provide evidence of high dissipation condition. We can calculate the difference between the maximum value of the dissipation and the value of  $Q3 + 1.5IQR$  of the distribution, which show the range of outlier in each distribution:

$$\Delta = D_{max} - (Q3 + 1.5IQR) \quad (20)$$

We plot  $\Delta$  in the two regimes in Fig.8.

With  $\Delta$  value, we believe that the greater range of the difference, the larger dissipation values of the distribution has. Thus, the high-dissipation phase has a greater value of  $\Delta$  than the low-dissipation phase.

Overall, the high-dissipation and low-dissipation conditions in our system are markedly distinct. In both scenarios, Langevin particles are driven by an external force from the massive vector field and dissipate their kinetic energy into the environment. However, under the low-dissipation condition, since  $m$ , which measures the cooperativity of the vectors, is significantly larger than  $J$ , indicative of the vectors' randomness, the vector configuration tends to differ from that of neighboring vectors. Consequently, most particles quickly become trapped at various fixed points before traveling far, resulting in shorter trajectories and less kinetic energy being dissipated into the system. On the other hand, in the high-dissipation condition,  $m$  and  $J$  are of comparable magnitude. This means vectors exhibit some degree of cooperativity with their neighbors, allowing more particles to travel greater distances and hop between fixed points, thus creating extensive trajectories. In this condition, there is a higher level of dissipation, particularly from particles that travel further than most others. This distinction is illustrated by the proportions (ratios) and ranges of relatively high dissipation for each condition, as shown in Fig.7 and Fig.8. In both figures, the range or ratio for the high dissipation condition is greater than that of the low dissipation condition. In conclusion, we can use both *Ratio* and  $\Delta$  as reliable indicators to determine whether the system is in the localized or delocalized phase.

## VI. CONCLUSION

In this work, we integrate the Langevin model with a massive vector field to simulate the behavior of random walks out of equilibrium under random drives. Our primary focus is on the particle trajectories and their energy dissipation, which occurs as the particles' kinetic energy is transferred to the environment while overcoming drag forces. Our numerical analysis confirms the existence of two distinct phases in our model: the low dissipation phase and the high dissipation phase. We introduce two metrics to diagnose these phases. We believe that our identification and characterization of these two dynamical phases will provide fundamental insights for understanding and manipulating nonequilibrium phases of matter. Looking ahead, we aim to investigate the scaling properties of dissipation within this model. We are also interested in exploring the relationship between dissipation and other thermodynamic quantities, such as configuration entropy. Ultimately, uncovering the complete phase diagram of the model represents a crucial future direction for our research.

## ACKNOWLEDGMENTS

Z.L. and J.Y. acknowledges support from Zhixin High School Science Outreach Program. Z.L. and J.Y. would

like to thank Weishun Zhong for suggesting this project, and guidance throughout carrying out the simulation and preparing this manuscript.

### Appendix A: Simulation parameters

In this section, we detail the parameter values used in the simulation. In our simulation, we discretize the lattice site of the massive vector field in Eqn.6 into 30 sites along each axes. The temperature of vector field in the Metropolis algorithm is set to be 0.15. The temperature of the Langevin system is 0.001. The simulation

time for massive vector field is 500 Monte-Carlo sweeps. We choose the time interval of discretizing the Langevin equation as 0.02 time units, and the total duration of the simulation is 500 time units. The drag coefficient in Eqn.13 is set to be  $\gamma=20$ . The size of the periodic box in the Langevin system is set to be 1. In all the simulations, we average over 1000 different initial conditions of the Langevin particles in each realization of the vector field, and average over 50 different realizations of the vector field to obtain the statistics presented in the main text.

- 
- [1] Christopher Jarzynski. Nonequilibrium equality for free energy differences. *Physical Review Letters*, 78(14):2690, 1997.
- [2] Gavin E Crooks. Entropy production fluctuation theorem and the nonequilibrium work relation for free energy differences. *Physical Review E*, 60(3):2721, 1999.
- [3] Udo Seifert. Stochastic thermodynamics, fluctuation theorems and molecular machines. *Reports on progress in physics*, 75(12):126001, 2012.
- [4] Arvind Murugan, Zorana Zeravcic, Michael P Brenner, and Stanislas Leibler. Multifarious assembly mixtures: Systems allowing retrieval of diverse stored structures. *Proceedings of the National Academy of Sciences*, 112(1):54–59, 2015.
- [5] Weishun Zhong, David J Schwab, and Arvind Murugan. Associative pattern recognition through macro-molecular self-assembly. *Journal of Statistical Physics*, 167:806–826, 2017.
- [6] Gili Bisker and Jeremy L England. Nonequilibrium associative retrieval of multiple stored self-assembly targets. *Proceedings of the National Academy of Sciences*, 115(45):E10531–E10538, 2018.
- [7] Jeremy L England. Statistical physics of self-replication. *The Journal of chemical physics*, 139(12):09B623\_1, 2013.
- [8] Marco Baiesi and Christian Maes. Life efficiency does not always increase with the dissipation rate. *Journal of Physics Communications*, 2(4):045017, 2018.
- [9] Carlos Floyd, Garegin A Papoian, and Christopher Jarzynski. Quantifying dissipation in actomyosin networks. *Interface focus*, 9(3):20180078, 2019.
- [10] Nikolay Perunov, Robert A Marsland, and Jeremy L England. Statistical physics of adaptation. *Physical Review X*, 6(2):021036, 2016.
- [11] Jeremy L England. Dissipative adaptation in driven self-assembly. *Nature nanotechnology*, 10(11):919–923, 2015.
- [12] Jordan M Horowitz and Jeremy L England. Spontaneous fine-tuning to environment in many-species chemical reaction networks. *Proceedings of the National Academy of Sciences*, 114(29):7565–7570, 2017.
- [13] Hridesh Kedia, Deng Pan, Jean-Jacques Slotine, and Jeremy L England. Drive-specific adaptation in disordered mechanical networks of bistable springs. *arXiv preprint arXiv:1908.09332*, 2019.
- [14] Jacob M Gold and Jeremy L England. Self-organized novelty detection in driven spin glasses. *arXiv preprint arXiv:1911.07216*, 2019.
- [15] Weishun Zhong, Jacob M Gold, Sarah Marzen, Jeremy L England, and Nicole Yunger Halpern. Quantifying many-body learning far from equilibrium with representation learning. *arXiv preprint arXiv:2001.03623*, 2020.
- [16] Weishun Zhong, Jacob M Gold, Sarah Marzen, Jeremy L England, and Nicole Yunger Halpern. Machine learning outperforms thermodynamics in measuring how well a many-body system learns a drive. *Scientific Reports*, 11(1):9333, 2021.
- [17] J-Ph Bouchaud, A Comtet, A Georges, and P Le Doussal. Classical diffusion of a particle in a one-dimensional random force field. *Annals of Physics*, 201(2):285–341, 1990.
- [18] Jean-Philippe Bouchaud and Antoine Georges. Anomalous diffusion in disordered media: statistical mechanisms, models and physical applications. *Physics reports*, 195(4-5):127–293, 1990.
- [19] Pawel Romanczuk, Markus Bär, Werner Ebeling, Benjamin Lindner, and Lutz Schimansky-Geier. Active brownian particles. *The European Physical Journal Special Topics*, 202(1):1–162, 2012.
- [20] Clemens Bechinger, Roberto Di Leonardo, Hartmut Löwen, Charles Reichhardt, Giorgio Volpe, and Giovanni Volpe. Active particles in complex and crowded environments. *Reviews of Modern Physics*, 88(4):045006, 2016.
- [21] Michael E Cates and Julien Tailleur. Motility-induced phase separation. *Annu. Rev. Condens. Matter Phys.*, 6(1):219–244, 2015.
- [22] Edward A Codling, Michael J Plank, and Simon Benhamou. Random walk models in biology. *Journal of the Royal society interface*, 5(25):813–834, 2008.
- [23] William Bialek. *Biophysics: searching for principles*. Princeton University Press, 2012.
- [24] Fred Solomon. Random walks in a random environment. *The annals of probability*, 3(1):1–31, 1975.
- [25] Andreas Greven and Frank den Hollander. Large deviations for a random walk in random environment. *The Annals of Probability*, 22(3):1381–1428, 1994.
- [26] Francesco Coghi, Jules Morand, and Hugo Touchette. Large deviations of random walks on random graphs. *Physical Review E*, 99(2):022137, 2019.
- [27] Giorgio Carugno, Pierpaolo Vivo, and Francesco Coghi. Delocalization-localization dynamical phase transition



- of random walks on graphs. *Physical Review E*, 107(2):024126, 2023.
- [28] Caterina De Bacco, Alberto Guggiola, Reimer Kühn, and Pierre Paga. Rare events statistics of random walks on networks: localisation and other dynamical phase transitions. *Journal of Physics A: Mathematical and Theoretical*, 49(18):184003, 2016.
- [29] David C Stuhmann and Francesco Coghi. Understanding random-walk dynamical phase coexistence through waiting times. *arXiv preprint arXiv:2308.03567*, 2023.
- [30] Jamir Marino, Martin Eckstein, Matthew S Foster, and Ana Maria Rey. Dynamical phase transitions in the collisionless pre-thermal states of isolated quantum systems: theory and experiments. *Reports on Progress in Physics*, 85(11):116001, 2022.
- [31] Scott Smale, Peiru He, Ben A Olsen, Kenneth G Jackson, Haille Sharum, Stefan Trotzky, Jamir Marino, Ana Maria Rey, and Joseph H Thywissen. Observation of a transition between dynamical phases in a quantum degenerate fermi gas. *Science Advances*, 5(8):eaax1568, 2019.
- [32] George E Uhlenbeck and Leonard S Ornstein. On the theory of the brownian motion. *Physical review*, 36(5):823, 1930.
- [33] Mark Srednicki. *Quantum field theory*. Cambridge University Press, 2007.
- [34] Mehran Kardar. *Statistical physics of fields*. Cambridge University Press, 2007.
- [35] H Eugene Stanley. Dependence of critical properties on dimensionality of spins. *Physical Review Letters*, 20(12):589, 1968.
- [36] Paul M Chaikin, Tom C Lubensky, and Thomas A Witten. *Principles of condensed matter physics*, volume 10. Cambridge university press Cambridge, 1995.
- [37] W Keith Hastings. Monte carlo sampling methods using markov chains and their applications. 1970.